

Article

Preparation and Superhydrophobicity of Nano-Al-Coated Wood by Magnetron Sputtering Based on Glow-Discharge Plasma

Zirun Xiao, Ruyi Ai, Yanan Wang, Liying Xu and Jingkui Li *

College of Science, Northeast Forestry University, Harbin 150040, China; xiao_zi_run@nefu.edu.cn (Z.X.); ary@nefu.edu.cn (R.A.); wang_ya_nan@nefu.edu.cn (Y.W.); 2022122962@nefu.edu.cn (L.X.)

* Correspondence: li_jing_kui@nefu.edu.cn

Abstract: A superhydrophobic coating on wood can effectively improve the hydrophobicity and service life of wood. In this study, an Al superhydrophobic nano-coating was constructed on the transversal section of poplar wood by magnetron sputtering based on glow-discharge plasma. The structure, microscopic morphology, surface elements, and hydrophobic properties were characterized and tested. When coated for 20 s, the water contact angle on the sample surface can reach 148.9°. When coated for 30 min, the Al-coated wood had a contact angle of 157.3°, which could maintain excellent superhydrophobic properties for 300 s. The sputtered Al nanoparticles were uniformly distributed on the wood surface and formed nanoclusters. Plenty of voids between the clusters can trap air and block contact between water droplets and the coating, making the coating obtain superhydrophobic properties. When the coating time was 60 min, the characteristic peak of the Al (111) crystal plane appeared at 38.4°, while the intensities of (101), (002), and (040) peaks of cellulose were reduced. In conclusion, magnetron sputtering was used to deposit a superhydrophobic coating on wood without low surface free energy agents. Furthermore, this research provides new inspirations for the physical modification of wood and the construction of superhydrophobic coatings on wood.

Keywords: glow-discharge plasma; magnetron sputtering; nano Al; superhydrophobicity



Citation: Xiao, Z.; Ai, R.; Wang, Y.; Xu, L.; Li, J. Preparation and Superhydrophobicity of Nano-Al-Coated Wood by Magnetron Sputtering Based on Glow-Discharge Plasma. *Forests* **2023**, *14*, 1761. <https://doi.org/10.3390/f14091761>

Academic Editor: Angela Lo Monaco

Received: 3 August 2023

Revised: 25 August 2023

Accepted: 28 August 2023

Published: 30 August 2023



Copyright: © 2023 by the authors. Licensee MDPI, Basel, Switzerland. This article is an open access article distributed under the terms and conditions of the Creative Commons Attribution (CC BY) license (<https://creativecommons.org/licenses/by/4.0/>).

1. Introduction

Wood, as a green and renewable material, is widely used in construction, paper making, furniture, and other fields [1,2]. Due to its abundant hydrophilic groups and natural porous structure, wood is prone to absorbing water, which can lead to deformation and cracking. Strong hydrophilicity can greatly reduce the service life and value of wood.

In recent years, superhydrophobic coatings have attracted extensive attention for their excellent properties such as water repellency, self-cleaning abilities [3], and surface protection [4]. These properties have potential applications in numerous areas such as mechanical components [5–7], aerospace [8], smart electronics [9], building materials [10], and medical treatments [11]. For example, aluminum-oxide-based coatings have been used in medical implants due to their superhydrophobic properties [12,13]. Superhydrophobic coatings on wood can not only enhance the appearance, texture, and decoration, but also provide desirable hydrophobicity for surface protection.

Many methods for preparing superhydrophobic coatings on wood surfaces have been broadly investigated. These methods include direct paint coating [14–20], lithography [21–24], hydrothermal methods [25,26], sol-gel methods [27–29], graft copolymerization [30,31], and layer-by-layer assembly [32–34]. With the deepening of research, a series of innovative processes and technologies have been gradually applied to the coating of wood surfaces. For example, Yin [35] et al. modified the surface of acetylated wood by chemical meteorological deposition (CVD) technology using trichloro silane (TCOS) to obtain a coating that can maintain superhydrophobic properties after a long time of

ultraviolet irradiation. Xie [36] et al. etched wood with oxygen plasma and then deposited a pentafluoroethane (PFE) film or diamond-like carbon (DLC) coating on the surface using a plasma deposition technique, resulting in a maximum contact angle of 161.2° on the wood surface. Inido [37] et al. prepared a polyester/TiO₂ coating on the wood surface using plasma spraying powder (PSP) and liquid precursor plasma spraying (LPPS) techniques, which imparted superhydrophobicity and anti-ultraviolet aging resistance to the wood surface.

These scholars have been exploring new processes for superhydrophobic coatings on wood with inspiring results. But most studies involve chemical reactions or use multiple chemical agents. By-products such as waste water and waste gas will be generated, endangering environmental safety and human health. In fact, several methods are available to achieve superhydrophobic properties without low-surface-energy agents on the surface of other materials. Specific methods include T-shape structures [38,39], oxygen vacancies [40], air trapped nanocavities [41], nanowires, and nanorods [42]. However, superhydrophobic coatings on wood surfaces without low-surface-energy chemical reagents are very difficult and poorly reported. For example, Bao [43] et al. prepared superhydrophobic Cu films on wood by magnetron sputtering but used low-surface-energy agents. Without low-surface-energy agents, superhydrophobic Cu, ITO, and Cu/CuO films have been realized on other materials by Li [44] et al., Gupta [45] et al., and An [42] et al., respectively. Magnetron sputtering is a physical vapor deposition (PVD) technique based on glow-discharge plasma, which can be used to prepare nanofilms through a bottom-up approach [46]. It has the merits of being pollution-free and having a low working temperature, easy scale production, and high film adhesion [47–49]. Magnetron sputtering is an indirect application of plasma, which is different from the general plasma surface treatment of wood. It is performed by bombarding the target with high-energy ions, causing the target atoms to sputter onto the substrate and form a nanofilm. No complex chemical reactions are involved in the process of magnetron sputtering, which is primarily a physical process. To the authors' knowledge, functional coatings on wood prepared by magnetron sputtering are still at an early stage [50,51].

In this article, magnetron sputtering was used to construct superhydrophobic coatings on the transverse section of poplar wood. This method does not use low-surface-energy chemical agents and is easy to produce on a large scale in the industry. It also provides new approaches for the physical modification of wood and the construction of superhydrophobic coatings on wood.

2. Materials and Methods

2.1. Test Materials

The wood samples were fast-growing poplar wood (*Populus sp.*, Linfen, Shanxi, China), which is accessible and an acceptable alternative to natural wood. The transverse section of the dried sapwood was machined into wood slices with the size of 25 mm × 25 mm × 2 mm (tangential × longitudinal × radial). The average density of the wood slices was 0.45 g/cm³. The moisture content of the wood slices was between 8% and 12%. Table 1 shows detailed information on the wood slices. The transverse surfaces had many exposed tubes and voids compared to the longitudinal surfaces. Coatings on transverse surfaces are more likely to become rough. The surfaces were sanded with sandpaper and were free of obvious defects, flaws, and mold. The purity of the aluminum (Al) target material was 99.99%, supplied by Beijing Zhongcheng New Material Technology Co., Ltd. (Beijing, China). Other materials included anhydrous ethanol, beakers, sandpaper, a knife, a steel ruler, and pressure-sensitive tape.

Table 1. Detailed information on the wood slices.

Density	Moisture Content	Size	Cutting Surface
0.45 g/cm ³	8%–12%	25 mm × 25 mm × 2 mm	transverse

2.2. Ultrasonic Pretreatment

The fast-growing poplar wood was pretreated with ultrasound as follows. The wood slices were placed in a beaker and fully submerged in anhydrous ethanol. A one-half volume of distilled water was added to an ultrasonic cleaner, and the beaker was placed into it. The switch was turned on to carry out the ultrasonic pretreatment for 30 min, and the poplar slices were removed with forceps. Finally, the wood was dried naturally to obtain the ultrasonicated poplar wood. Ultrasonic pretreatment can effectively remove dust, gum, and other impurities from the wood surface, which exposes more pores. Different material treatments and fabrication processes would result in different material properties and performances [52,53]. Other methods such as soaking, polishing, and grinding can also be used to remove the impurities. It is beneficial for aluminum nanoparticles to form a superhydrophobic surface with a certain degree of roughness.

2.3. Preparation of the Al-Coated Wood

The Al nano-coatings were deposited on the wood via a JGP-450 type multi-target magnetron sputtering equipment (Sky Technology Development Co., Ltd., Shenyang, China). The sputtering target was an aluminum target (99.999% purity) and the substrate was poplar wood with ultrasonic pretreatment. The whole sputtering process was divided into several steps such as installing the wood slices, pumping at a low vacuum, pumping at a high vacuum, and sputtering the Al. Firstly, the samples and Al target were installed, then the container was closed and the mechanical pump was turned on to pump at a low vacuum. Next, when the vacuum reached 2.0 Pa, the resistance vacuum gauge was switched off while the molecular pump was turned on to pump at a high vacuum. When the vacuum level reached 8.0×10^{-4} Pa, the ionization vacuum gauge was shut off. Then, argon gas was injected and the sputtering pressure and argon flow rate were controlled at 3.0 Pa and 20 sccm, respectively. Finally, the direct current (DC) power supply was switched on with a sputtering power of 50 W. Due to the uneven fibers on the wood surface, the edges of the coating are difficult to distinguish when the coating time is short. The thickness of the Al coating deposited on the wood surface was controlled by changing the sputtering time (20 s, 50 s, 15 min, 30 min, 60 min). When the deposition time is short, the coating is non-continuous and only strong hydrophobicity can be realized. Superhydrophobicity can only be achieved when the coating time is long (the nanoparticles completely cover the wood). Figure 1 shows a diagram of a nano-Al superhydrophobic coating on wood prepared by magnetron sputtering.

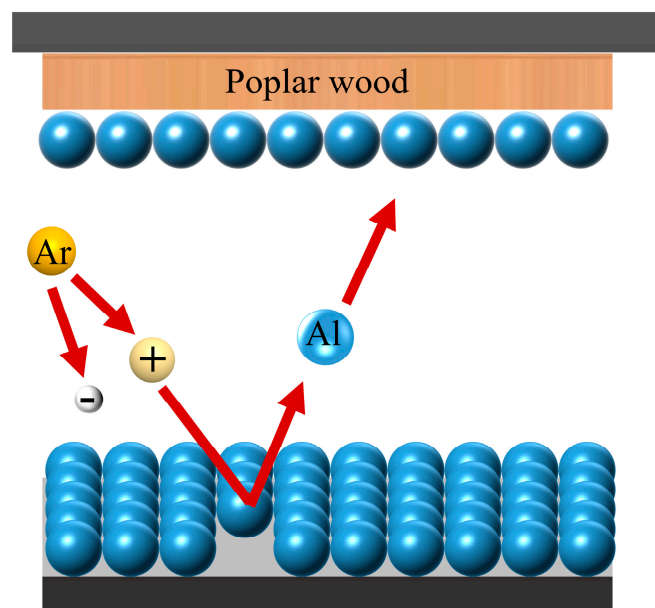


Figure 1. Nano-Al superhydrophobic coating on wood prepared by magnetron sputtering.

2.4. Characterization

2.4.1. Structure

The structure of the wood was characterized by an X-ray diffractometer (XRD-6100) manufactured by Shimadzu Corporation, Kyoto, Japan. The scanning range was 5°–85° with a scanning speed of 4°/min. The voltage and current of the X-ray tube were 40 kV and 30 mA, respectively.

2.4.2. Static and Dynamic Hydrophobic Properties

The water contact angle (WCA) of the wood was measured with an SDC-350 contact angle meter (Dongguan Shengding Precision Instrument Co., Ltd., Dongguan, China). The droplet volume was set to 5 μ L. Five different locations on the sample surface were randomly selected for testing.

2.4.3. Fourier Infrared Spectrum

The surface functional groups were analyzed using an iS10 Fourier infrared spectrometer (ATR-FTIR, Thermo Fisher, Waltham, MA, USA). The acquisition range was set from 500 to 4000/cm, and the sampling frequency was 16 times.

2.4.4. Microscopic Morphology

The surface morphology was characterized using a JSM-7500F cold-field emission scanning electron microscope (SEM, JEOL, Tokyo, Japan).

2.4.5. Surface Fluorescence Effect

The surface fluorescence properties were characterized using a DXM-1200F fluorescence microscope (Nikon, Tokyo, Japan) at a magnification of 200 times.

2.4.6. Surface Element Content and Distribution

The elemental composition and distribution of the wood surface were analyzed using an Oxford X-Max electric cooling energy spectrometer (EDS, Oxford, UK).

2.4.7. Surface Element Valence

The elemental valence of the wood was analyzed using a K-Alpha type X-ray photoelectron spectrometer (XPS, Thermo Fisher Scientific, Waltham, MA, USA). The X-ray was measured with a beam diameter of 200 μ m and a power of 100 W.

3. Results and Analysis

3.1. Structure Analysis

The X-ray diffraction (XRD) technique is used to analyze the crystallography of objects through the peaks formed [54]. Figure 2 shows the XRD pattern of the Al-coated wood. Three characteristic peaks of (101), (002), and (040) were detected in the transverse sections of the wood, which belong to cellulose type I [55,56]. Specifically, the transverse section of the wood had a selective orientation of the (040) crystal plane, so that a very sharp diffraction peak of the (040) crystal plane can be observed at 34.4°. When the coating time was 60 min, the characteristic peak of the Al appeared at 2 θ of 38.4°, which is the typical face-centered cubic structure of the metal Al (111) crystal plane. This indicates that the Al nanoparticles were deposited onto the wood surface, forming a nanofilm with a (111) crystal plane preferred orientation. The Al (111) crystal plane has the lowest surface energy compared with other Al crystal planes [57], and its selective orientation may affect the hydrophobicity of the coating [42]. In addition, the three characteristic peaks of cellulose were still present when Al nanoparticles were sputtered for 60 min, suggesting that the deposition of the Al nano-coating by magnetron sputtering did not alter the natural structure of the wood. The decrease in the intensity of the diffraction peaks was mainly due to the reduction of the X-ray radiation depth caused by the Al coating.

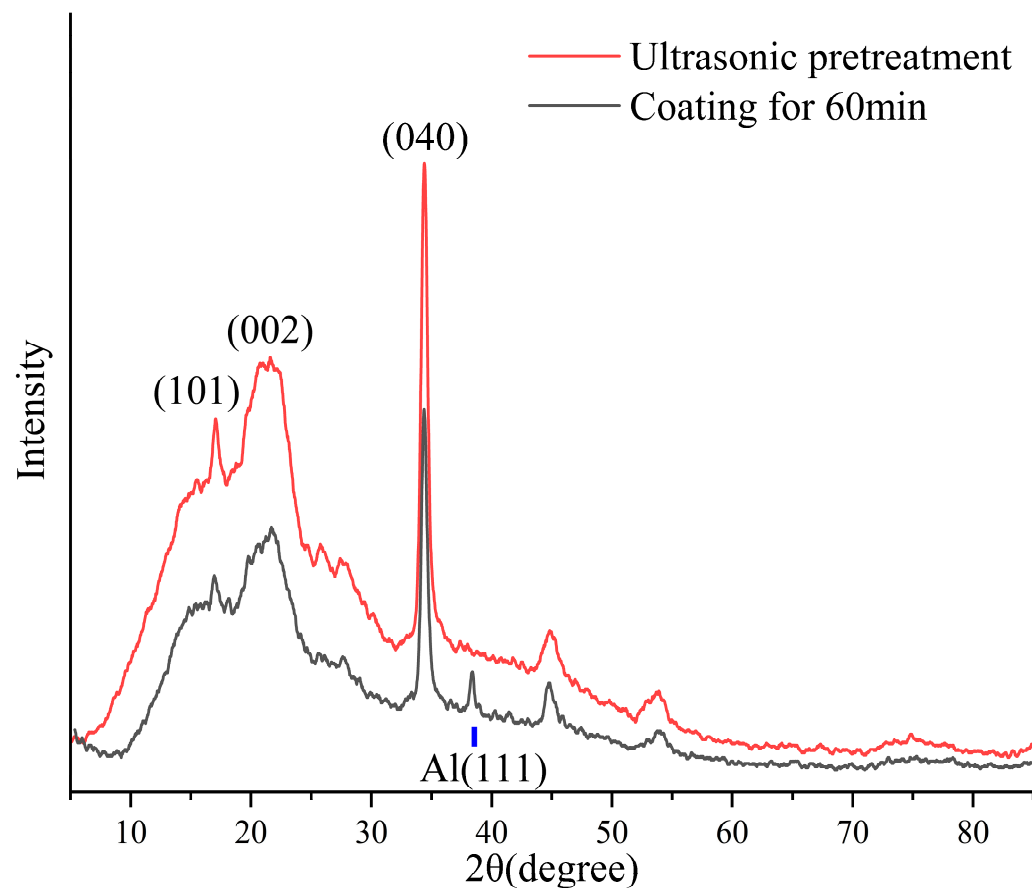


Figure 2. XRD pattern of the Al-coated wood.

3.2. Static Hydrophobic Performance Analysis

Figure 3 shows the static hydrophobic performance of the Al-coated wood. The water contact angle was measured when water droplets were dropped on the cross-cut wood slices for 15 s. The droplets on the ultrasonicated wood showed a flattened shape with a contact angle of 18.8° , exhibiting strong hydrophilicity. The contact angle (CA) was 148.9° for the sample with a coating time of 20 s. And when the coating time was 50 s, the contact angle was 149.5° , which was close to being superhydrophobic. At this time, parts of the functional groups on the wood surface were covered by a small number of sputtered Al nanoparticles, and the surface wettability turned from hydrophilic to strongly hydrophobic. When coated with Al for 15 min, the contact angle was 150.1° , which just reached the superhydrophobic angle. In general, the hydrophobicity of superhydrophobic coatings is associated with surface roughness. A rougher surface implies better superhydrophobic properties. The cross-sectional surface of the ultrasonicated wood was distributed with lots of exposed openings and pores, which are conducive to the preparation of a superhydrophobic surface [58]. With the increase of sputtering time, a large number of Al nanoparticles were attached to the wood fibers. The attachment reduced the contact area between solid and liquid, which resulted in superhydrophobic properties on the wood surface [59–61]. When sputtered for 30 min, the contact angle reached 157.3° after the droplets remained for 15 s, showing excellent superhydrophobic performance. The contact angle was 156.4° for the wood with a sputtering time of 60 min. This was similar to the sample that was sputtered for 30 min, which still exhibited stable superhydrophobic properties.

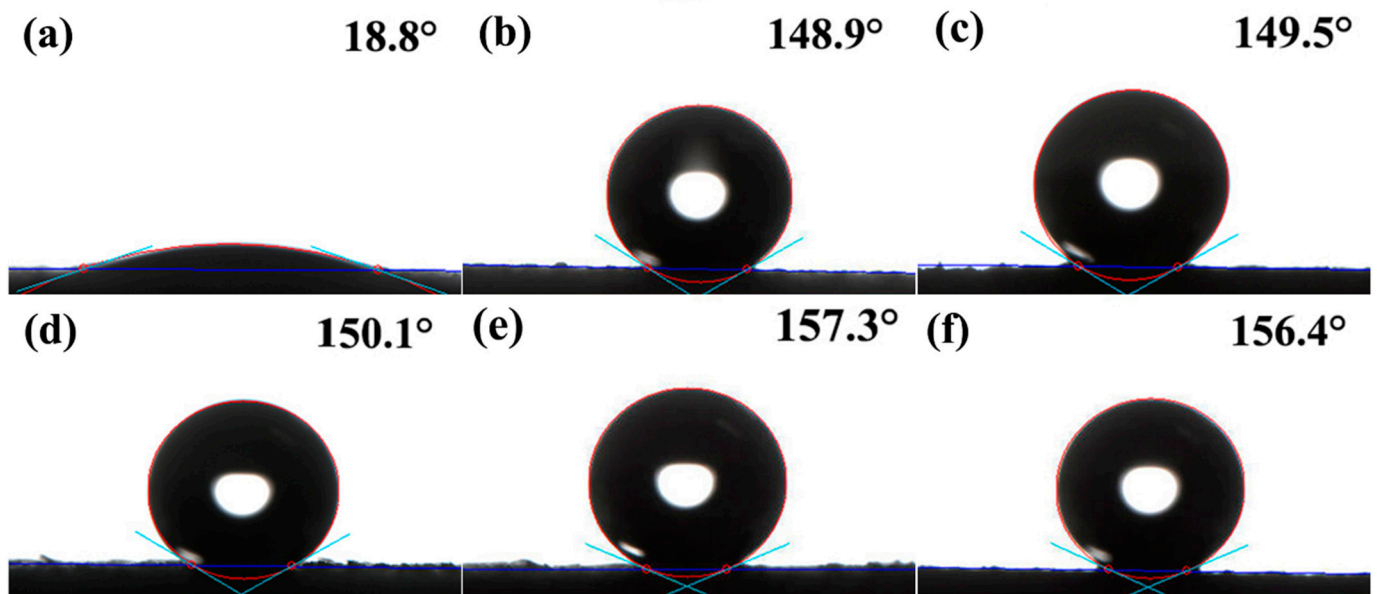


Figure 3. Static hydrophobic performance of the Al-coated wood: (a) ultrasonic pretreatment; (b) coating for 20 s; (c) coating for 50 s; (d) coating for 15 min; (e) coating for 30 min; (f) coating for 60 min.

3.3. Dynamic Wettability Analysis

Figure 4 shows the dynamic wettability of the Al-coated wood. The contact angle was measured when the water droplets were kept on the wood surface for 3 s, 15 s, 30 s, 60 s, 90 s, 120 s, 240 s, and 300 s. The poplar wood with ultrasonic pretreatment exhibited strong water absorption, and the droplet on the wood was completely absorbed within 30 s. There are two main reasons for the strong hygroscopicity. The first is the absorption of water by the abundant capillary structure on the cross-section of the porous wood; the second is the rapid combination of polar functional groups such as hydroxyl groups (-OH) which are distributed on the cellulose amorphous region, hemicellulose, and lignin of the wood with water molecules in the form of hydrogen bonds. With a sputtering time of 20 s, the water contact angle can be maintained above 140° for 120 s. After that, the contact angle decreased quickly and dropped to 114.2° after 300 s. This was attributed to the fact that only a small number of Al nanoparticles were sputtered onto the wood surface, which could not completely cover the hydrophilic groups to prevent the binding with water. When the sputtering time was 50 s, the water contact angle was above 140° for 300 s, which maintained a strong hydrophobicity. With this sputtering time, the hydrophilic functional groups on the wood surface were basically covered by more sputtered Al nanoparticles, and the hydrophobicity was enhanced. With the increase of sputtering time, the contact angle of the wood coated for 15 min was 146.3° after the droplet remained for 300 s, which had better water stability than the wood coated for 50 s. However, the contact angle still declined below 150° after holding for 30 s and could not maintain the superhydrophobic performance for a long time. This was because the sputtering time was not long enough and the deposited Al nano-coating had tiny gaps and cracks so that water molecules could penetrate into the coating through the micro-cracks. When the coating time was 30 min and 60 min, the samples had contact angles larger than 150° for 300 s of droplet retention, indicating they could maintain the superhydrophobic properties over a long period. The results indicated that when a continuous nanofilm with a certain roughness was formed on the wood surface, the wettability of the sample surface tended to be stable.

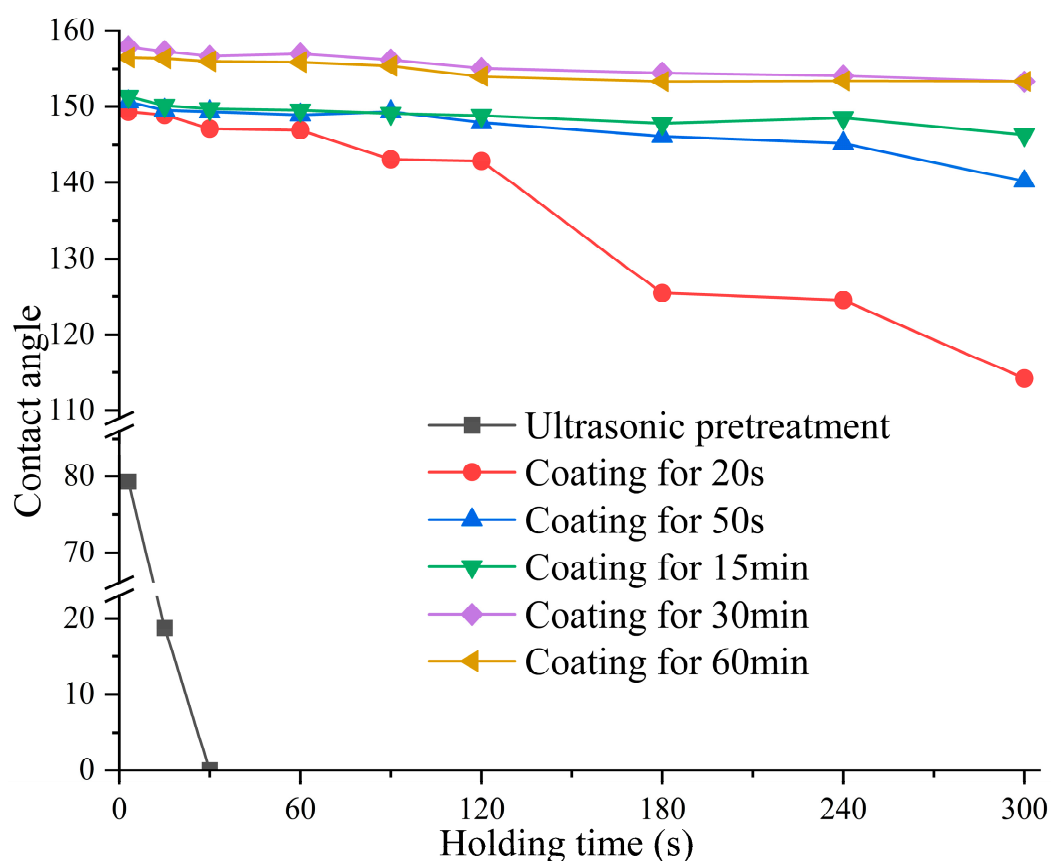


Figure 4. Dynamic wettability of the Al-coated wood.

3.4. Adhesion Analysis

Figure 5 shows the adhesion behavior between the droplets and coating sputtered for 30 min. The 5 μ L water droplet carried by the syringe was compressed, deformed, and lifted when it touched the superhydrophobic surface. The water droplet could maintain its full shape when it touched the wood surface, and could be easily removed from the coating surface without droplet residue. It strongly demonstrated the superhydrophobicity and low adhesion of the Al nano-coating. In addition, the process of water droplets impacting wood may be further investigated by computational simulation. Computational simulation has the advantages of low cost and fast results [62–64]. In accordance with the ISO2409 [65] international standard, the adhesion between coating and wood was tested by the scratching method. The coating was cut into 2 mm \times 2 mm sized grids by a knife and then torn with pressure-sensitive tape. Figure 6 shows pictures of the wood before and after the coating–wood adhesion test. The coatings in the squares were generally intact, and there were almost no coating flakes at the edges of the squares. The average adhesion level of the coating was level 1; a very good adhesion for daily use.

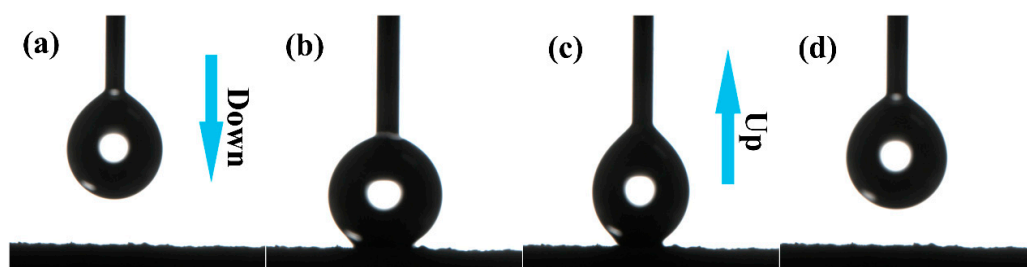


Figure 5. Adhesion behavior between droplet and coating sputtered for 30 min: (a) down; (b) contact; (c) up; (d) separate.

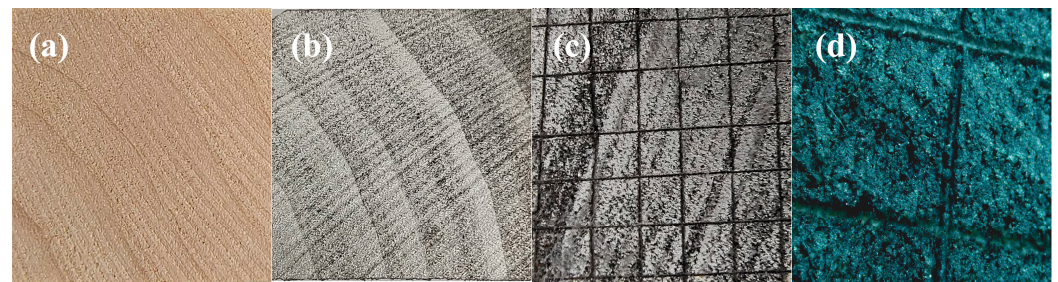


Figure 6. Adhesion between coating and wood: (a) ultrasonic pretreatment; (b) coating for 60 min; (c) wood coated for 60 min after adhesion testing; (d) observation at 40 times magnification after testing.

3.5. Infrared Spectrum Analysis

Figure 7 shows the Fourier infrared spectrum (FTIR) of the Al-coated wood. In the wood samples, the characteristic peak at 3345 cm^{-1} is the O-H stretching vibration. The absorption peaks at 2936 cm^{-1} and 2872 cm^{-1} are mainly attributed to the C-H stretching vibrations of methyl ($-\text{CH}_3$) and methylene ($-\text{CH}_2$). The feature peak at 1030 cm^{-1} belongs to the C-O stretching vibration. As the sputtering time increased, the intensity of the infrared characteristic peaks of the wood gradually decreased, and the most obvious decreases were observed at 3345 cm^{-1} and 1030 cm^{-1} . When the coating time was 20 s or 50 s, the clear absorption peaks of the natural wood were still visible. The Al nanoparticles did not completely cover the groups on the wood surface. When the coating time reached 15 min, the characteristic peaks of the natural wood were close to disappearing, indicating that a continuous Al nanofilm had been formed. When the sputtering time was 30 min or 60 min, the characteristic peaks disappeared totally and the infrared curve of the sample was a smooth curve. This means that the Al nanofilms were well deposited on the wood surface and the thickness reached a certain level, which blocked the infrared absorption. In addition, for the samples coated with Al, the peaks of hydrophilic groups such as the hydroxyl groups at 3330 cm^{-1} (O-H) and carbonyl groups at 1735 cm^{-1} ($\text{C}=\text{O}$) diminished in intensity, which also confirmed the transition of the samples from hydrophilic to hydrophobic.

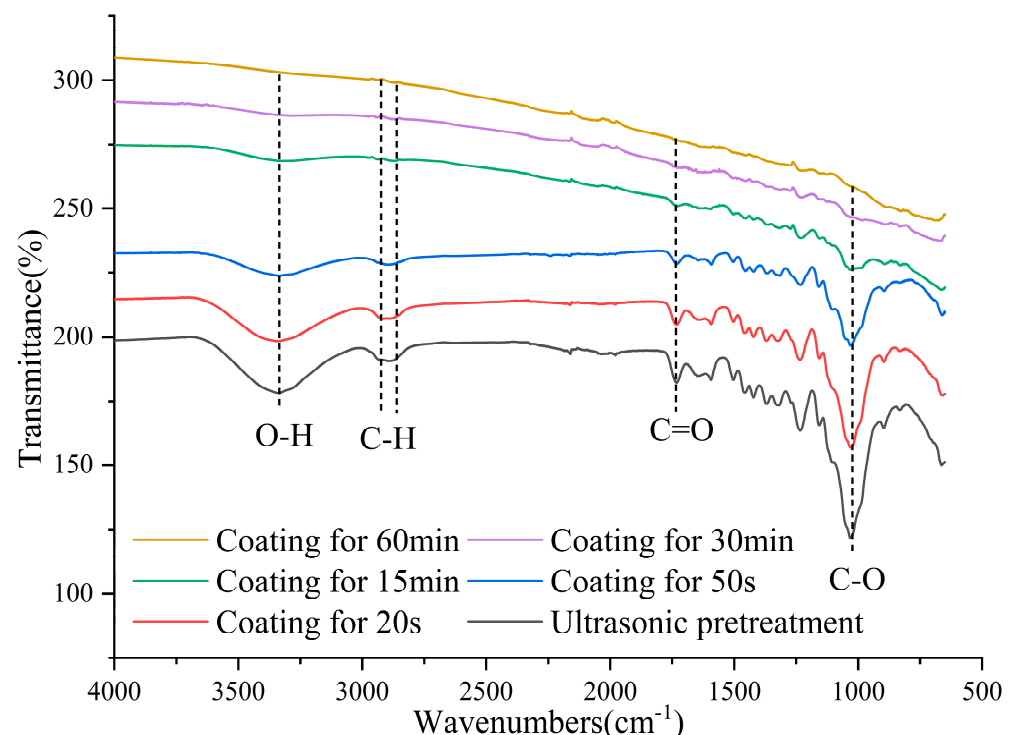


Figure 7. Fourier infrared spectrum of the Al-coated wood.

3.6. Microscopic Morphology Analysis

Figure 8 shows the microscopic morphology of the Al-coated wood. Due to the ultrasonic cavitation effect, massive tiny bubbles burst to form blast waves that continuously struck the wood. The amorphous deposits and intrusive fillers were effectively removed. It can be observed that the cross-section of the ultrasonicated wood is very uneven, with fibers, pits, and grooves on the surface. When the coating time was 20 s, only a small number of nanoparticles were deposited on the surface, and the fibers and pores on the poplar surface were still clearly visible. When the coating time was 50 s, the fibers on the wood surface were adhered to by the Al nanoparticles, while plenty of Al nanoparticles penetrated deeply into the pores and ravines. The wood surface became relatively flat because the pores and ravines were further filled. When coated for 15 min, the wood was already covered with Al nanofilm such that the natural structure of the wood could not be observed. At this point, the nanofilm was in the island growth period and there were still tiny gaps in the growing film. When coated with Al for 30 min, there were more Al nanoparticles aggregating to form clusters on the sample surface and the growth of the Al nano-coating was more complete. The nanoclusters were clearly visible on the surface of the Al-coated fibers under high magnification. There were an enormous number of irregular vacancies between the nanoclusters, in which lots of air was trapped. In this way, the contact between water droplets and the coatings can be blocked [66], enabling the coatings to obtain superhydrophobic properties. As the sputtering time reached 60 min, the coating thickness was approximately 45 μm . A massive number of Al nanoparticles densely covered the wood fibers, forming a rough surface with micro–nano structures. In addition, Al-coated surfaces with micro–nano structures may absorb organic compounds in the air. The spontaneous adsorption of hydrocarbons could modify the coating surface and reduce its surface free energy, making the surface superhydrophobic [67,68].

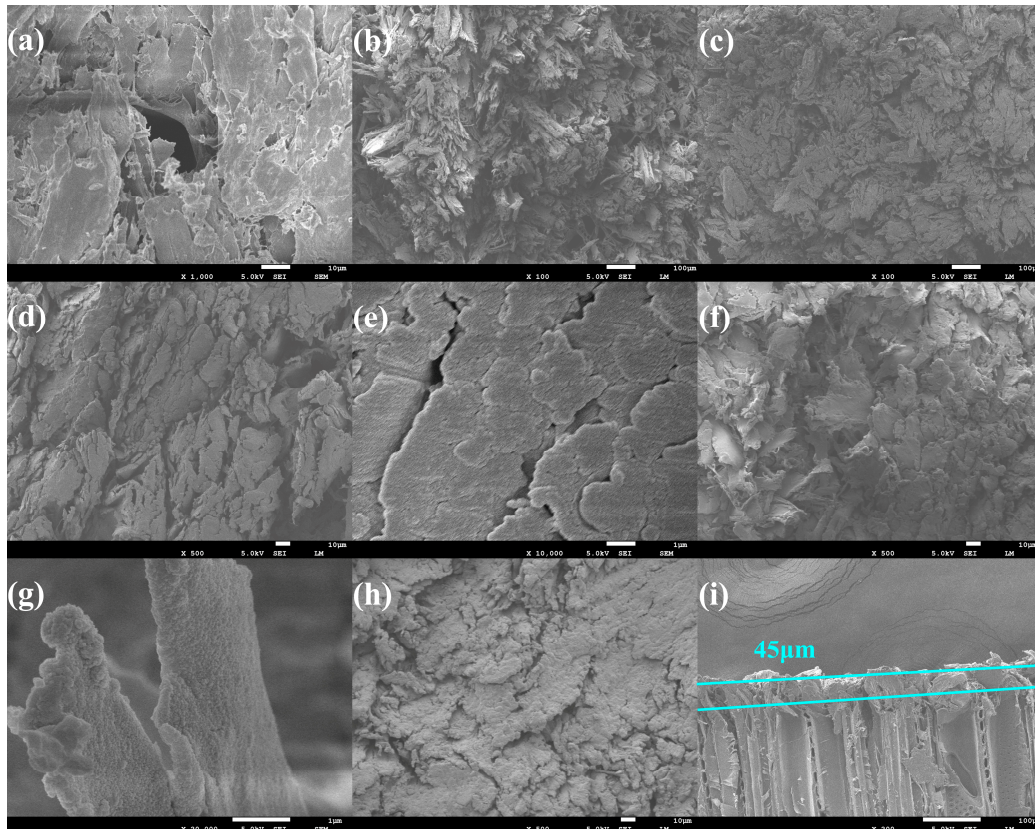


Figure 8. Microscopic morphology of the Al-coated wood: (a) ultrasonic pretreatment; (b) coating for 20 s; (c) coating for 50 s; (d,e) coating for 15 min; (f,g) coating for 30 min; (h) coating for 60 min; (i) coating thickness with a coating time of 60 min.

3.7. Surface Fluorescence Effect Analysis

Figure 9 shows the surface fluorescence effect of the Al-coated wood. Wood can emit a natural blue fluorescence under ultraviolet irradiation because of the lignin [69,70]. With ultrasonic pretreatment, the original wood surface was removed of impurities such as dust and gum, so that pores and transport tissues were exposed. When the coating time was 20 s, only a few Al particles were deposited on the wood surface. The wood still showed light blue fluorescence and the tubular pore structure was clearly visible. When the coating time was 50 s, more Al nanoparticles were attached to the wood fibers and covered some of the fluorescent groups. The fluorescence became dim and appeared dark blue, while a few tube-hole tissues could be observed. When the sputtering time was 15 min, most areas in the visual field appeared blue–black. At this time, many Al nanoparticles covered the wood and formed a nano-coating, which prevented the natural fluorescence produced by lignin. However, there were many gullies, pits, and holes in the transverse section of the ultrasonicated wood, and the sputtered Al atoms penetrated deeply into them without forming a continuous film, so the blue–black areas were not continuous. When the coating time reached 30 min and 60 min, the field of view basically turned black. The Al nanofilms completely covered the wood surface, forming continuous Al nanofilms.

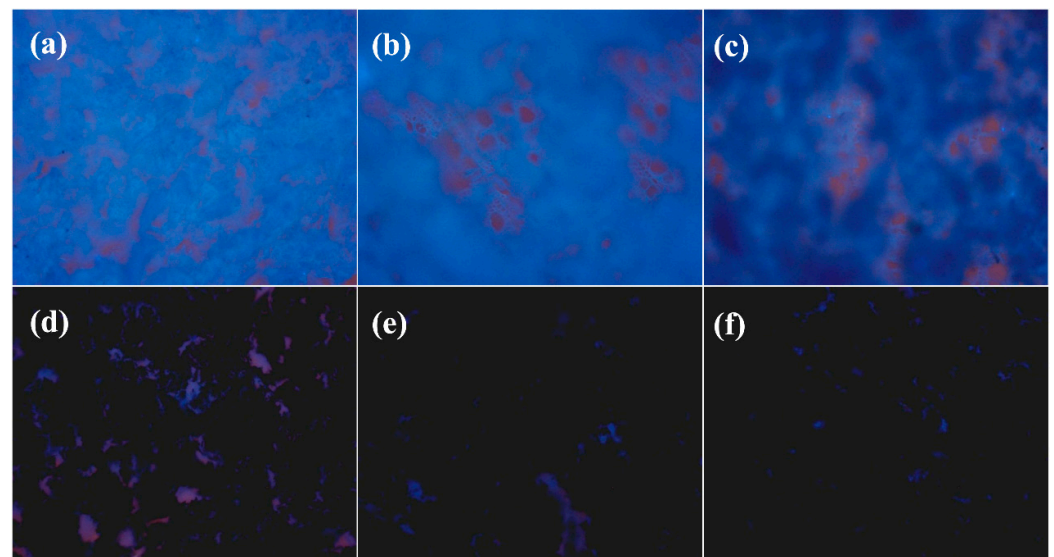


Figure 9. Al nano-coating growth on cross-sectional wood under a fluorescence microscope (200 times): (a) ultrasonic pretreatment; (b) coating for 20 s; (c) coating for 50 s; (d) coating for 15 min; (e) coating for 30 min; (f) coating for 60 min.

3.8. Surface Element Content and Distribution Analysis

Figure 10 shows the energy-dispersive X-ray spectra (EDS) map of the Al-coated wood. Table 2 shows the weight percentages of the surface elements of the samples. The H element could not be detected by EDS owing to its light mass and low molecular weight. On the uncoated wood, C and O elements could only be detected at 0.277 eV and 0.525 eV with relative content of 51.26% and 48.74%, respectively. When the Al nanoparticles were coated on the wood, the three elements C, O, and Al were detected on the surface. The relative content of the three elements varied with the sputtering time. In the five groups of samples with sputtering times of 20 s, 50 s, 15 min, 30 min, and 60 min, the weight percentages of the Al element were 1.20%, 2.24%, 10.62%, 13.70%, and 26.59%, respectively. The weight percentages of the C element were 52.38%, 50.22%, 45.72%, 45.77%, and 31.05%, and the weight percentages of the O element were 46.42%, 47.54%, 43.65%, 40.53%, and 42.37%, respectively. It can be seen that the content of the Al element was relatively low and the contents of the C and O elements were relatively high when coated with Al for 20 s and 50 s. The results indicated that fewer Al nanoparticles were deposited on the surface of the poplar wood, and the nanofilms grew slowly. As the coating time increased, more

Al nanoparticles were deposited on the wood surface and the thickness of the formed Al nanofilms also increased. When the coating time was 15 min and 30 min, the relative content of the Al element was detected to increase gradually, while the relative contents of the C and O elements were reduced. When the sputtering time was 60 min, the number of Al nanoparticles deposited on the wood surface was the largest. The ratio of the C and O elements declined obviously, and the relative content of Al reached the maximum. The surface was covered with Al nanoparticles, forming a uniform and dense nanofilm.

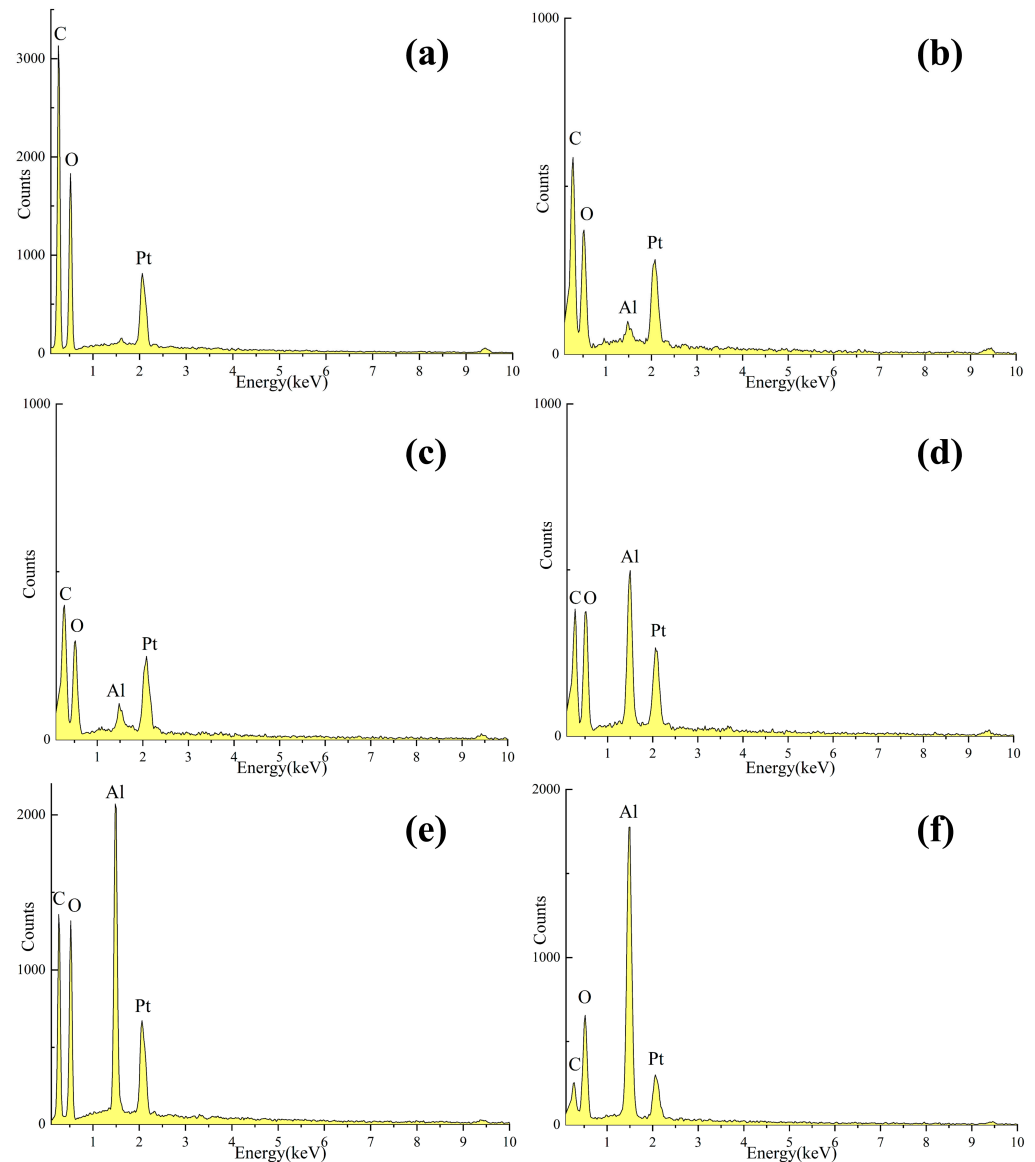


Figure 10. EDS map of the Al-coated wood: (a) ultrasonic pretreatment; (b) coating for 20 s; (c) coating for 50 s; (d) coating for 15 min; (e) coating for 30 min; (f) coating for 60 min.

Table 2. Weight percentages of surface elements.

Element	Ultrasonic Pretreatment	Coating for 20 s	Coating for 50 s	Coating for 15 min	Coating for 60 min	Coating for 60 min
C	51.26%	52.38%	50.22%	45.72%	45.77%	31.05%
O	48.74%	46.42%	47.54%	43.65%	40.53%	42.37%
Al	-	1.20%	2.24%	10.62%	13.70%	26.59%

"-" means no or no value detected.

Figure 11 shows the overall distribution of Al elements on the Al-coated wood at 200 times magnification. When the coating time was 20 s and 50 s, the distribution of Al nanoparticles on the surfaces was sparse due to the short coating time. As the coating time increased, with a coating time of 15 min and 30 min, more uniformly distributed Al nanoparticles could be seen on the surfaces of the wood. When the coating time reached 60 min, the content of the Al element on the wood surface was the highest, and a great number of Al nanoparticles uniformly covered the sample surface and formed a nano-coating.

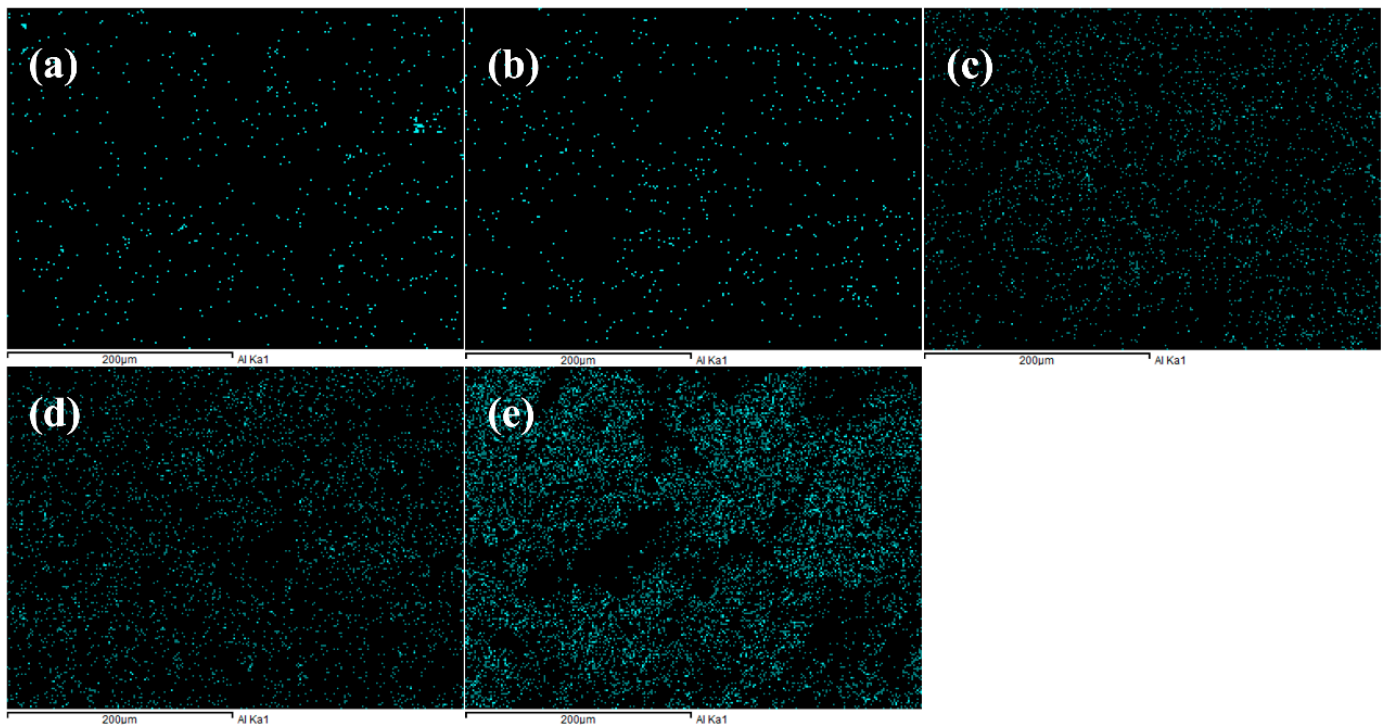


Figure 11. The overall distribution of the Al element on the Al-coated wood at 200 times magnification: (a) coating for 20 s; (b) coating for 50 s; (c) coating for 15 min; (d) coating for 30 min; (e) coating for 60 min.

3.9. Surface Element Valence Analysis

Figure 12 shows the X-ray photoelectron spectroscopy (XPS) of the Al-coated wood. The distinctive peaks of C1s, O1s, Al2s, and Al2p appeared in the full spectrum of the wood coated for 15 min. As shown in Figure 10b, the detected Al element was present in the oxidation state when the sputtering time was 20 s [71]. This is mainly because few Al nanoparticles were deposited on the wood and almost all of them were oxidized by air. When the sputtering time was 50 s, the valence state of the elemental metal Al was detected besides the oxide of Al. This was because the outermost layer of the nanofilm was oxidized. The penetration depth of XPS is generally from 3 to 10 nm, so the electrons of the metal Al in the interior could be excited. After a long sputtering period, the deposited coatings were mainly composed of metal Al, with many zero-valent Al nanoparticles present in the interior. When the coating time was 15 min, 30 min, and 60 min, it was observed that the content of zero-valent Al was rising with the increase in coating time. It was demonstrated that the dense outer Al-oxide protective layer could block the contact of the internal metal Al with oxygen. Therefore, a large number of Al nanoparticles could be successfully deposited onto the wood without being oxidized. In a word, the XPS analysis showed that the deposited nanofilms were composed of zero-valent Al and surface oxide layers.

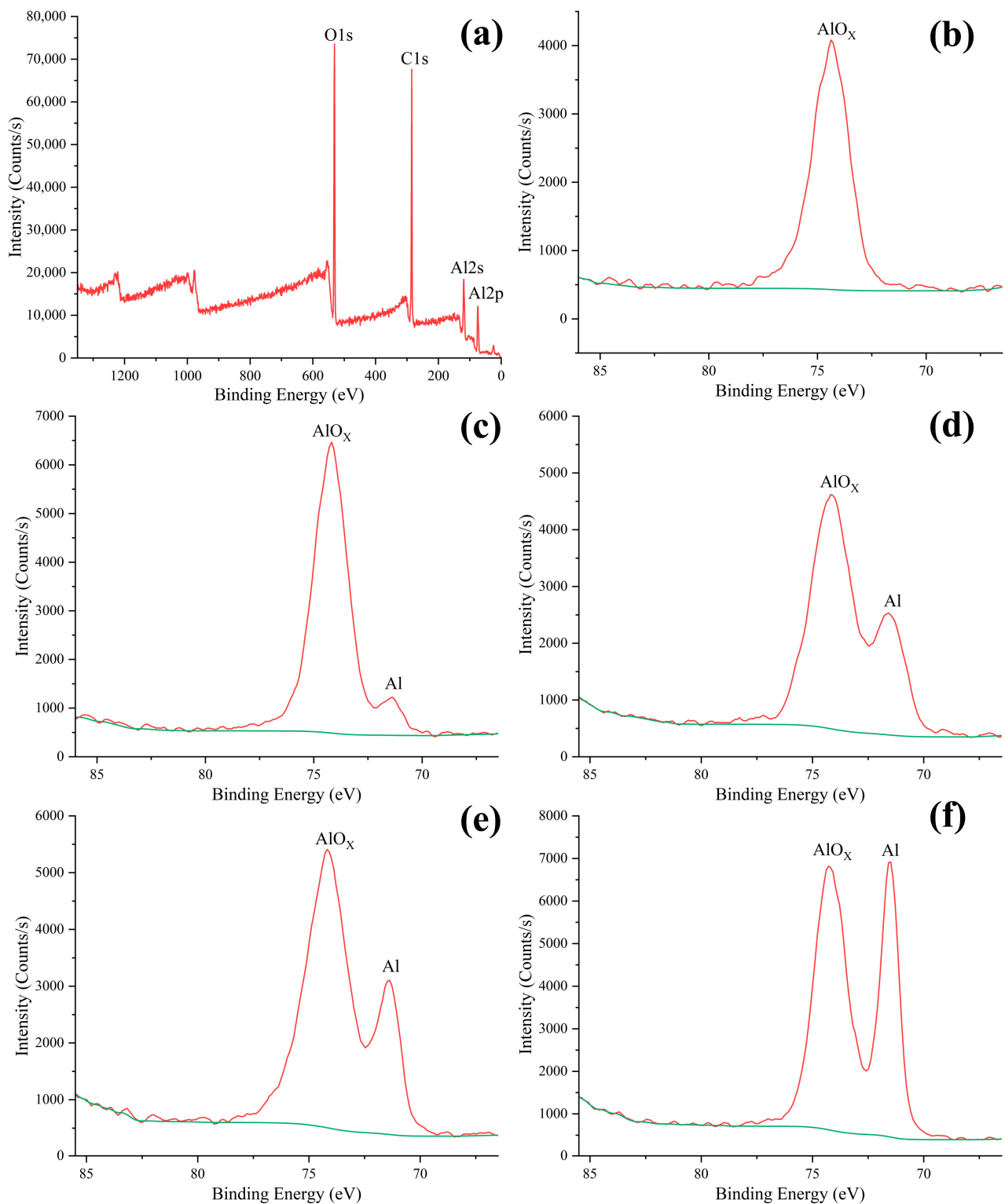


Figure 12. XPS pattern for the Al-coated wood: (a) full spectrum of the wood coated for 15 min; (b) coating for 20 s; (c) coating for 50 s; (d) coating for 15 min; (e) coating for 30 min; (f) coating for 60 min.

4. Conclusions

This research set out to construct superhydrophobic Al nano-coatings on the transversal sections of fast-growing wood by an environment-friendly magnetron sputtering process. The transversal section of ultrasonicated wood is distributed with many natural pores,

holes, and grooves, which is conducive to the formation of the superhydrophobic coating. The sputtered Al atoms were aggregated into nanoclusters and uniformly distributed on the wood surface, to form a superhydrophobic coating with a preferred orientation of the Al (111) crystal plane. When the coating time was 30 min, the superhydrophobic coating had low adhesion without adhering to droplets. Meanwhile, the contact angle could be maintained at about 157° within 60 s of droplet contact, and a long-term superhydrophobic effect could be maintained for 300 s. When coated for 60 min, the infrared characteristic peaks of the wood completely disappeared and the Al element content on the surface reached 26.59%. In addition, the XPS analysis showed that the outer layer of the nano-coating was oxidized to a dense layer of aluminum oxide, preventing the continued oxidation of the inner metal Al. Magnetron sputtering is a physical vapor deposition technology based on glow-discharge plasma, which is pollution-free and easy to produce on a large scale. However, preparation is still in the exploratory stage for superhydrophobic coatings on wood prepared by magnetron sputtering. Specialized equipment is required to produce the coating, and the cost will be reduced to an acceptable level with large-scale production. The abrasion resistance, anti-ice, and anti-corrosion properties of superhydrophobic coatings also need to be studied in the future. In conclusion, this article has constructed nano-Al coatings on wood by magnetron sputtering without low-surface-energy agents, which provides a feasible method for the study of the composite of inorganic nanomaterials and wood, and also provides a new research idea for the construction of superhydrophobic coatings on wood surfaces.

Author Contributions: Conceptualization, Z.X. and J.L.; methodology, Z.X.; experimental part, Z.X., R.A. and J.L.; formal analysis, R.A. and Y.W.; investigation, R.A., Y.W. and L.X.; data analysis, Z.X., Y.W. and L.X.; literature search, R.A., Y.W. and L.X.; writing—original draft preparation, Z.X.; writing—review and editing, J.L. All authors have read and agreed to the published version of the manuscript.

Funding: This work was supported by the Fundamental Research Funds for the Central Universities (2572023DJ01).

Data Availability Statement: Data are available upon request due to privacy or ethical restrictions. Data from this study are available from the corresponding authors upon request. Because of the privacy implications of the data in this study, these data are not publicly available.

Conflicts of Interest: The authors declare no conflict of interest.

References

1. Song, J.; Chen, C.; Zhu, S.; Zhu, M.; Dai, J.; Ray, U.; Li, Y.; Kuang, Y.; Li, Y.; Quispe, N.; et al. Processing Bulk Natural Wood into a High-Performance Structural Material. *Nature* **2018**, *554*, 224–228. [[CrossRef](#)] [[PubMed](#)]
2. Tuong, V.M.; Huyen, N.V.; Kien, N.T.; Dien, N.V. Durable Epoxy@ZnO Coating for Improvement of Hydrophobicity and Color Stability of Wood. *Polymers* **2019**, *11*, 1388. [[CrossRef](#)] [[PubMed](#)]
3. Hooda, A.; Goyat, M.S.; Pandey, J.K.; Kumar, A.; Gupta, R. A Review on Fundamentals, Constraints and Fabrication Techniques of Superhydrophobic Coatings. *Prog. Org. Coat.* **2020**, *142*, 105557. [[CrossRef](#)]
4. Fan, X.; Song, S.; Shi, Y.; Cai, M.; Huang, Y.; Zhang, B.; Zhu, M. Mechanochemical Stable Superhydrophobic Coating toward Lasting Corrosion Protection. *Prog. Org. Coat.* **2023**, *178*, 107478. [[CrossRef](#)]
5. Boinovich, L.B.; Domantovskii, A.G.; Emelyanenko, A.M.; Miller, A.B.; Potapov, Y.F.; Khodan, A.N. Antiicing Performance of Superhydrophobic Coatings on Aluminum and Stainless Steel. *Russ Chem Bull* **2013**, *62*, 380–387. [[CrossRef](#)]
6. Dong, S.; Wang, Z.; An, L.; Li, Y.; Wang, B.; Ji, H.; Wang, H. Facile Fabrication of a Superhydrophobic Surface with Robust Micro-/Nanoscale Hierarchical Structures on Titanium Substrate. *Nanomaterials* **2020**, *10*, 1509. [[CrossRef](#)]
7. Yang, S.; Luo, S.; Yang, L.; Yang, X. A Durable Superhydrophobic Surface with Protective Nest-like Micro-Containers. *Mater. Today Commun.* **2022**, *33*, 104460. [[CrossRef](#)]
8. Sun, Y.; Wang, Y.; Liang, W.; He, L.; Wang, F.; Zhu, D.; Zhao, H. In Situ Activation of Superhydrophobic Surfaces with Triple Icephobicity at Low Temperatures. *ACS Appl. Mater. Interfaces* **2022**, *14*, 49352–49361. [[CrossRef](#)]
9. Dong, J.; Wang, D.; Peng, Y.; Zhang, C.; Lai, F.; He, G.; Ma, P.; Dong, W.; Huang, Y.; Parkin, I.P.; et al. Ultra-Stretchable and Superhydrophobic Textile-Based Bioelectrodes for Robust Self-Cleaning and Personal Health Monitoring. *Nano Energy* **2022**, *97*, 107160. [[CrossRef](#)]

10. Zulfiqar, U.; Awais, M.; Hussain, S.Z.; Hussain, I.; Husain, S.W.; Subhani, T. Durable and Self-Healing Superhydrophobic Surfaces for Building Materials. *Mater. Lett.* **2017**, *192*, 56–59. [[CrossRef](#)]
11. Luo, J.; Yu, H.; Lu, B.; Wang, D.; Deng, X. Superhydrophobic Biological Fluid-Repellent Surfaces: Mechanisms and Applications. *Small Methods* **2022**, *6*, 2201106. [[CrossRef](#)]
12. Haidar, A.; Ali, A.A.; Veziroglu, S.; Fiutowski, J.; Eichler, H.; Mueller, I.; Kiefer, K.; Faupel, F.; Bischoff, M.; Veith, M.; et al. PTFEP-Al₂O₃ Hybrid Nanowires Reducing Thrombosis and Biofouling. *Nanoscale Adv.* **2019**, *1*, 4659–4664. [[CrossRef](#)] [[PubMed](#)]
13. Ammarullah, M.I.; Santoso, G.; Sugiharto, S.; Supriyono, T.; Wibowo, D.B.; Kurdi, O.; Tauviqirrahman, M.; Jamari, J. Minimizing Risk of Failure from Ceramic-on-Ceramic Total Hip Prosthesis by Selecting Ceramic Materials Based on Tresca Stress. *Sustainability* **2022**, *14*, 13413. [[CrossRef](#)]
14. Xu, L.; Karunakaran, R.G.; Guo, J.; Yang, S. Transparent, Superhydrophobic Surfaces from One-Step Spin Coating of Hydrophobic Nanoparticles. *ACS Appl. Mater. Interfaces* **2012**, *4*, 1118–1125. [[CrossRef](#)] [[PubMed](#)]
15. Shah, S.M.; Zulfiqar, U.; Hussain, S.Z.; Ahmad, I.; Habib-ur-Rehman; Hussain, I.; Subhani, T. A Durable Superhydrophobic Coating for the Protection of Wood Materials. *Mater. Lett.* **2017**, *203*, 17–20. [[CrossRef](#)]
16. Yao, Y.; Gellerich, A.; Zauner, M.; Wang, X.; Zhang, K. Differential Anti-Fungal Effects from Hydrophobic and Superhydrophobic Wood Based on Cellulose and Glycerol Stearoyl Esters. *Cellulose* **2018**, *25*, 1329–1338. [[CrossRef](#)]
17. Huang, J.; Wang, S.; Lyu, S.; Fu, F. Preparation of a Robust Cellulose Nanocrystal Superhydrophobic Coating for Self-Cleaning and Oil-Water Separation Only by Spraying. *Ind. Crop. Prod.* **2018**, *122*, 438–447. [[CrossRef](#)]
18. Zhao, X.; Park, D.S.; Choi, J.; Park, S.; Soper, S.A.; Murphy, M.C. Robust, Transparent, Superhydrophobic Coatings Using Novel Hydrophobic/Hydrophilic Dual-Sized Silica Particles. *J. Colloid Interface Sci.* **2020**, *574*, 347–354. [[CrossRef](#)]
19. Zhan, K.; Lu, Q.; Xia, S.; Guo, C.; Zhao, S.; Gao, W.; Yang, L.; Morrell, J.J.; Yi, T.; Xie, L.; et al. A Cost Effective Strategy to Fabricate STA@PF@Cu₂O Hierarchical Structure on Wood Surface: Aimed at Superhydrophobic Modification. *Wood Sci. Technol.* **2021**, *55*, 565–583. [[CrossRef](#)]
20. Wang, Z.; Sun, Z.; Chen, X.; Zou, W.; Jiang, X.; Sun, D.; Yu, M. Color Fastness Enhancement of Dyed Wood by Si-Sol@PDMS Based Superhydrophobic Coating. *Colloids Surf. A Physicochem. Eng. Asp.* **2022**, *651*, 129701. [[CrossRef](#)]
21. Chen, Y.; Wang, H.; Yao, Q.; Fan, B.; Wang, C.; Xiong, Y.; Jin, C.; Sun, Q. Biomimetic Taro Leaf-like Films Decorated on Wood Surfaces Using Soft Lithography for Superparamagnetic and Superhydrophobic Performance. *J. Mater. Sci.* **2017**, *52*, 7428–7438. [[CrossRef](#)]
22. Bao, W.; Liang, D.; Zhang, M.; Jiao, Y.; Wang, L.; Cai, L.; Li, J. Durable, High Conductivity, Superhydrophobicity Bamboo Timber Surface for Nanoimprint Stamps. *Prog. Nat. Sci. Mater. Int.* **2017**, *27*, 669–673. [[CrossRef](#)]
23. Yang, Y.; He, H.; Li, Y.; Qiu, J. Using Nanoimprint Lithography to Create Robust, Buoyant, Superhydrophobic PVB/SiO₂ Coatings on Wood Surfaces Inspired by Red Roses Petal. *Sci. Rep.* **2019**, *9*, 9961. [[CrossRef](#)] [[PubMed](#)]
24. Yang, Y.; Shen, H.; Qiu, J. Fabrication of Biomimetic Robust Self-Cleaning Superhydrophobic Wood with Canna-Leaf-like Micro/Nanostructure through Morph-Genetic Method Improved Water-, UV-, and Corrosion Resistance Properties. *J. Mol. Struct.* **2020**, *1219*, 128616. [[CrossRef](#)]
25. Makarona, E.; Koutzagiotti, C.; Salmas, C.; Ntalos, G.; Skoulikidou, M.-C.; Tsamis, C. Enhancing Wood Resistance to Humidity with Nanostructured ZnO Coatings. *Nano-Struct. Nano-Objects* **2017**, *10*, 57–68. [[CrossRef](#)]
26. Lu, Q.; Cheng, R.; Jiang, H.; Xia, S.; Zhan, K.; Yi, T.; Morrell, J.J.; Yang, L.; Wan, H.; Du, G.; et al. Superhydrophobic Wood Fabricated by Epoxy/Cu₂(OH)₃Cl NPs/Stearic Acid with Performance of Desirable Self-Cleaning, Anti-Mold, Dimensional Stability, Mechanical and Chemical Durability. *Colloids Surf. A Physicochem. Eng. Asp.* **2022**, *647*, 129162. [[CrossRef](#)]
27. Tsvetkova, I.N.; Krasil'nikova, L.N.; Khoroshavina, Y.V.; Galushko, A.S.; Yu, V.F.; Kychkin, A.K.; Shilova, O.A. Sol-Gel Preparation of Protective and Decorative Coatings on Wood. *J. Sol-Gel Sci. Technol.* **2019**, *92*, 474–483. [[CrossRef](#)]
28. Xia, M.; Yang, T.; Chen, S.; Yuan, G. Fabrication of Superhydrophobic Eucalyptus Wood Surface with Self-Cleaning Performance in Air and Oil Environment and High Durability. *Colloid Interface Sci. Commun.* **2020**, *36*, 100264. [[CrossRef](#)]
29. Wang, Y.; Ge-Zhang, S.; Mu, P.; Wang, X.; Li, S.; Qiao, L.; Mu, H. Advances in Sol-Gel-Based Superhydrophobic Coatings for Wood: A Review. *Int. J. Mol. Sci.* **2023**, *24*, 9675. [[CrossRef](#)]
30. Wang, Y.; Tang, Z.; Lu, S.; Zhang, M.; Liu, K.; Xiao, H.; Huang, L.; Chen, L.; Wu, H.; Ni, Y. Superhydrophobic Wood Grafted by Poly(2-(Perfluorooctyl)Ethyl Methacrylate) via ATRP with Self-Cleaning, Abrasion Resistance and Anti-Mold Properties. *Holzforschung* **2020**, *74*, 799–809. [[CrossRef](#)]
31. Sharma, G.; Kumar, A.; Naushad, M.; Al-Misned, F.A.; El-Serehy, H.A.; Ghfar, A.A.; Rai Sharma, K.; Si, C.; Stadler, F.J. Graft Copolymerization of Acrylonitrile and Ethyl Acrylate onto *Pinus Roxburghii* Wood Surface Enhanced Physicochemical Properties and Antibacterial Activity. *J. Chem.* **2020**, *2020*, e6285354. [[CrossRef](#)]
32. Lu, X.; Hu, Y. Layer-by-Layer Deposition of TiO₂ Nanoparticles in the Wood Surface and Its Superhydrophobic Performance. *BioResources* **2016**, *11*, 4605–4620. [[CrossRef](#)]
33. Wan, Y.; Hou, S.; Guo, M.; Fu, Y. Surface Properties of Spray-Assisted Layer-By-Layer ElectroStatic Self-Assembly Treated Wooden Take-Off Board. *Appl. Sci. Basel* **2021**, *11*, 836. [[CrossRef](#)]
34. Shao, C.; Jiang, M.; Zhang, J.; Zhang, Q.; Han, L.; Wu, Y. Construction of a Superhydrophobic Wood Surface Coating by Layer-by-Layer Assembly: Self-Adhesive Properties of Polydopamine. *Appl. Surf. Sci.* **2023**, *609*, 155259. [[CrossRef](#)]
35. Yin, H.; Moghaddam, M.S.; Tuominen, M.; Dédinaité, A.; Wälinder, M.; Swerin, A. Wettability Performance and Physicochemical Properties of UV Exposed Superhydrophobized Birch Wood. *Appl. Surf. Sci.* **2022**, *584*, 152528. [[CrossRef](#)]

36. Xie, L.; Tang, Z.; Jiang, L.; Breedveld, V.; Hess, D.W. Creation of Superhydrophobic Wood Surfaces by Plasma Etching and Thin-Film Deposition. *Surf. Coat. Technol.* **2015**, *281*, 125–132. [[CrossRef](#)]
37. Jnido, G.; Ohms, G.; Vioel, W. One-Step Deposition of Polyester/TiO₂ Coatings by Atmospheric Pressure Plasma Jet on Wood Surfaces for UV and Moisture Protection. *Coatings* **2020**, *10*, 184. [[CrossRef](#)]
38. Hoshian, S.; Jokinen, V.; Somerkivi, V.; Lokanathan, A.R.; Franssila, S. Robust Superhydrophobic Silicon without a Low Surface-Energy Hydrophobic Coating. *ACS Appl. Mater. Interfaces* **2015**, *7*, 941–949. [[CrossRef](#)]
39. Yang, C.; Cui, S.; Weng, Y.; Wu, Z.; Liu, L.; Ma, Z.; Tian, X.; Fu, R.K.Y.; Chu, P.K.; Wu, Z. Scalable Superhydrophobic T-Shape Micro/Nano Structured Inorganic Alumina Coatings. *Chem. Eng. J.* **2021**, *409*, 128142. [[CrossRef](#)]
40. Qi, G.; Liu, X.; Li, C.; Wang, C.; Yuan, Z. The Origin of Superhydrophobicity for Intrinsically Hydrophilic Metal Oxides: A Preferential O₂ Adsorption Dominated by Oxygen Vacancies. *Angew. Chem. Int. Ed.* **2019**, *58*, 17406–17411. [[CrossRef](#)]
41. Sahoo, P.; Dhara, S.; Dash, S.; Raj, B.; Manna, I.; Tyagi, A.K. Air Trapped Nanocavity Induced Superhydrophobicity on GaN Microbelt. *Appl. Phys. Lett.* **2011**, *98*, 043103. [[CrossRef](#)]
42. An, X.; Yang, C.; Wu, Z.; Liu, L.; Li, S.; Zhou, L.; Tang, W.; Ma, Z.; Wu, Z.; Fu, R.K.Y.; et al. Self-Regulated Super-Hydrophobic Cu/CuO Electrode Film Deposited by One-Step High-Power Sputtering. *Adv. Electron. Mater.* **2020**, *6*, 1900891. [[CrossRef](#)]
43. Bao, W.; Zhang, M.; Jia, Z.; Jiao, Y.; Cai, L.; Liang, D.; Li, J. Cu Thin Films on Wood Surface for Robust Superhydrophobicity by Magnetron Sputtering Treatment with Perfluorocarboxylic Acid. *Eur. J. Wood Wood Prod.* **2019**, *77*, 115–123. [[CrossRef](#)]
44. Li, G.; Wang, B.; Liu, Y.; Tan, T.; Song, X.; Li, E.; Yan, H. Stable Superhydrophobic Surface: Fabrication of Interstitial Cottonlike Structure of Copper Nanocrystals by Magnetron Sputtering. *Sci. Technol. Adv. Mater.* **2008**, *9*, 025006. [[CrossRef](#)]
45. Gupta, N.; Sasikala, S.; Mahadik, D.B.; Rao, A.V.; Barshilia, H.C. Dual-Scale Rough Multifunctional Superhydrophobic ITO Coatings Prepared by Air Annealing of Sputtered Indium-Tin Alloy Thin Films. *Appl. Surf. Sci.* **2012**, *258*, 9723–9731. [[CrossRef](#)]
46. Abid, N.; Khan, M.; Shujait, S.; Chaudhary, K.; Ikram, M.; Imran, M.; Haider, J.; Khan, M.; Khan, Q.; Maqbool, M. Synthesis of Nanomaterials Using Various Top-down and Bottom-up Approaches, Influencing Factors, Advantages, and Disadvantages: A Review. *Adv. Colloid Interface Sci.* **2022**, *300*, 102597. [[CrossRef](#)]
47. Sarakinos, K.; Alami, J.; Konstantinidis, S. High Power Pulsed Magnetron Sputtering: A Review on Scientific and Engineering State of the Art. *Surf. Coat. Technol.* **2010**, *204*, 1661–1684. [[CrossRef](#)]
48. Wan, C.; Jiao, Y.; Li, J. A Cellulose Fibers-Supported Hierarchical Forest-like Cuprous Oxide/Copper Array Architecture as a Flexible and Free-Standing Electrode for Symmetric Supercapacitors. *J. Mater. Chem. A* **2017**, *5*, 17267–17278. [[CrossRef](#)]
49. Liang, J.; Liu, Q.; Li, T.; Luo, Y.; Lu, S.; Shi, X.; Zhang, F.; Asiri, A.M.; Sun, X. Magnetron Sputtering Enabled Sustainable Synthesis of Nanomaterials for Energy Electrocatalysis. *Green Chem.* **2021**, *23*, 2834–2867. [[CrossRef](#)]
50. Wang, Y.; Wu, X.; Wang, Y.; Tian, Y.; Mu, H.; Li, J. Hydrophobic and UV-Resistant Properties of Environmentally Friendly Nano-ZnO-Coated Wood. *Holzforschung* **2021**, *75*, 138–147. [[CrossRef](#)]
51. Xiao, Z.; Wang, Y.; Song, Y.; Li, Q.; Xu, Q.; Li, J. Functional Improvement of Fast-Growing Wood Based on Nano-ZnO/PDMS Double-Layer Structure. *Wood Sci. Technol.* **2023**, *57*, 275–288. [[CrossRef](#)]
52. Anand, P.B.; Nagaraja, S.; Jayaram, N.; Sreenivasa, S.P.; Almakayee, N.; Khan, T.M.Y.; Kumar, R.; Ammarullah, M.I. Kenaf Fiber and Hemp Fiber Multi-Walled Carbon Nanotube Filler-Reinforced Epoxy-Based Hybrid Composites for Biomedical Applications: Morphological and Mechanical Characterization. *J. Compos. Sci.* **2023**, *7*, 324. [[CrossRef](#)]
53. Mughal, K.; Mughal, M.P.; Farooq, M.U.; Anwar, S.; Ammarullah, M.I. Using Nano-Fluids Minimum Quantity Lubrication (NF-MQL) to Improve Tool Wear Characteristics for Efficient Machining of CFRP/Ti6Al4V Aeronautical Structural Composite. *Processes* **2023**, *11*, 1540. [[CrossRef](#)]
54. Santoso, B.; Ammarullah, M.I.; Haryati, S.; Sofijan, A.; Bustan, M.D. Power and Energy Optimization of Carbon Based Lithium-Ion Battery from Water Spinach (*Ipomoea aquatica*). *J. Ecol. Eng.* **2023**, *24*, 213–223. [[CrossRef](#)]
55. Jiang, B.; Chen, C.; Liang, Z.; He, S.; Kuang, Y.; Song, J.; Mi, R.; Chen, G.; Jiao, M.; Hu, L. Lignin as a Wood-Inspired Binder Enabled Strong, Water Stable, and Biodegradable Paper for Plastic Replacement. *Adv. Funct. Mater.* **2020**, *30*, 1906307. [[CrossRef](#)]
56. Yu, S.; Liu, Z.; Xu, N.; Chen, J.; Gao, Y. Influencing Factors for Determining the Crystallinity of Native Cellulose by X-Ray Diffraction. *Anal. Sci.* **2020**, *36*, 947–951. [[CrossRef](#)]
57. Li, R.; Zhong, Y.; Huang, C.; Tao, X.; Ouyang, Y. Surface Energy and Surface Self-Diffusion of Al Calculated by Embedded Atom Method. *Physica B* **2013**, *422*, 51–55. [[CrossRef](#)]
58. Wu, Y.; Jia, S.; Wang, S.; Qing, Y.; Yan, N.; Wang, Q.; Meng, T. A Facile and Novel Emulsion for Efficient and Convenient Fabrication of Durable Superhydrophobic Materials. *Chem. Eng. J.* **2017**, *328*, 186–196. [[CrossRef](#)]
59. Zhang, W.; Wang, D.; Sun, Z.; Song, J.; Deng, X. Robust Superhydrophobicity: Mechanisms and Strategies. *Chem. Soc. Rev.* **2021**, *50*, 4031–4061. [[CrossRef](#)]
60. He, Y.; Wang, L.; Wu, T.; Wu, Z.; Chen, Y.; Yin, K. Facile Fabrication of Hierarchical Textures for Substrate-Independent and Durable Superhydrophobic Surfaces. *Nanoscale* **2022**, *14*, 9392–9400. [[CrossRef](#)]
61. Li, X.; Gao, L.; Wang, M.; Lv, D.; He, P.; Xie, Y.; Zhan, X.; Li, J.; Lin, Z. Recent Development and Emerging Applications of Robust Biomimetic Superhydrophobic Wood. *J. Mater. Chem. A* **2023**, *11*, 6772–6795. [[CrossRef](#)]
62. Liu, C.; Zhu, L.; Bu, W.; Liang, Y. Superhydrophobic Surfaces: From Nature to Biomimetic through VOF Simulation. *Micron* **2018**, *107*, 94–100. [[CrossRef](#)] [[PubMed](#)]

63. Ammarullah, M.I.; Afif, I.Y.; Maula, M.I.; Winarni, T.I.; Tauviqirrahman, M.; Akbar, I.; Basri, H.; van der Heide, E.; Jamari, J. Tresca Stress Simulation of Metal-on-Metal Total Hip Arthroplasty during Normal Walking Activity. *Materials* **2021**, *14*, 7554. [[CrossRef](#)] [[PubMed](#)]
64. Ammarullah, M.I.; Hartono, R.; Supriyono, T.; Santoso, G.; Sugiharto, S.; Permana, M.S. Polycrystalline Diamond as a Potential Material for the Hard-on-Hard Bearing of Total Hip Prosthesis: Von Mises Stress Analysis. *Biomedicines* **2023**, *11*, 951. [[CrossRef](#)] [[PubMed](#)]
65. Banos, O.; Bergmann, U.; Glorius, M.; Ohmann, S.; Seidel, T.; Breikopf, C. New Preparation Methods for Coated Heat Exchangers in Adsorption Refrigeration and Heat Pumps Applications. *Sci Rep* **2022**, *12*, 8004. [[CrossRef](#)]
66. Cui, M.; Shen, Y.; Tian, H.; Yang, Y.; Feng, H.; Li, J. Influence of Water Adhesion of Superhydrophobic Surfaces on Their Anti-Corrosive Behavior. *Surf. Coat. Technol.* **2018**, *347*, 38–45. [[CrossRef](#)]
67. Liu, P.; Cao, L.; Zhao, W.; Xia, Y.; Huang, W.; Li, Z. Insights into the Superhydrophobicity of Metallic Surfaces Prepared by Electrodeposition Involving Spontaneous Adsorption of Airborne Hydrocarbons. *Appl. Surf. Sci.* **2015**, *324*, 576–583. [[CrossRef](#)]
68. Yan, X.; Chen, F.; Zhang, X.; Qin, Y.; Zhao, C.; Sett, S.; Cha, H.; Hoque, M.J.; Zhao, F.; Huang, Z.; et al. Atmosphere-Mediated Scalable and Durable Biphilicity on Rationally Designed Structured Surfaces. *Adv. Mater. Interfaces* **2020**, *7*, 2000475. [[CrossRef](#)]
69. Donaldson, L. Softwood and Hardwood Lignin Fluorescence Spectra of Wood Cell Walls in Different Mounting Media. *IAWA J.* **2013**, *34*, 3–19. [[CrossRef](#)]
70. Xue, Y.; Qiu, X.; Ouyang, X. Insights into the Effect of Aggregation on Lignin Fluorescence and Its Application for Microstructure Analysis. *Int. J. Biol. Macromol.* **2020**, *154*, 981–988. [[CrossRef](#)]
71. Reddy, I.N.; Reddy, V.R.; Dey, A.; Sridhara, N.; Basavaraja, S.; Bera, P.; Anandan, C.; Sharma, A.K. Microstructural Studies of E-Beam Evaporated Alumina Thin Films. *Surf. Eng.* **2014**, *30*, 594–599. [[CrossRef](#)]

Disclaimer/Publisher's Note: The statements, opinions and data contained in all publications are solely those of the individual author(s) and contributor(s) and not of MDPI and/or the editor(s). MDPI and/or the editor(s) disclaim responsibility for any injury to people or property resulting from any ideas, methods, instructions or products referred to in the content.